Integration of Dual-Arm Manipulation in a Passivity Based Whole-Body Controller for Torque-Controlled Humanoid Robots

Juan Miguel Garcia-Haro[1], Bernd Henze[2], George Mesesan[2], Santiago Martinez[1] and Christian Ott[2]

***Abstract*— This work presents an extension of balance control for torque-controlled humanoid robots. Within a non-strict task hierarchy, the controller allows the robot to use the feet end-effectors to balance, while the remaining hand end-effectors can be used to perform Dual-Arm manipulation. The controller generates a passive and compliance behaviour to regulate the location of the centre of mass (CoM), the orientation of the hip and the poses of each end-effector assigned to the task of interaction (in this case bi-manipulation). Then, an appropriate wrench (force and torque) is applied to each of the end-effectors employed for the task to achieve this purpose. Now, in this new controller, the essential requirement focuses on the fact that the desired wrench in the CoM is computed through the sum of the balancing and bi-manipulation wrenches. The bi-manipulation wrenches are obtained through a new dynamic model that allows executing tasks of approaching the grip and manipulation of large objects compliantly. On the other hand, the feedback controller has been maintained but in combination with a bi-manipulation-oriented feedforward control to improve the performance in the object trajectory tracking. This controller is tested in different experiments with the robot TORO.**

Fig. 1. The humanoid robot TORO transporting objects on a tray.

I. INTRODUCTION

The essential behaviour of a humanoid robot should have the capacity to keep stability and also walk (compliantly) with the application of possible external perturbations. Sensitive compliance and impedance control can be achieved via joint torque sensing and control [1]. Torque-sensing has been applied in some humanoid robots like Valikyrie [2], in which its joint architecture eliminates the additional noise in both position and torque sensing to improve the control. At the Institute of Robotics and Mechatronics of DLR, the humanoid robot TORO has been developed using the joint technology of the DLR-KUKA Light-Weight Robot, which can be operated both in torque or position mode [3].

More complex methodologies are implemented when using a whole-body control approach. For instance, a whole-body nonlinear model predictive control approach for rigid body systems subject to contacts is presented in [4]. By the use of a contact model as part of the whole-dynamic system, the approach is able to optimize the location, sequence, and timings of the contacts efficiently.

This project has received funding from the European Research Council (ERC) (grant agreement No. 819358), from the HUMASOFT (DPI2016-75330-P) and RoboCity2030-DIH-CM (S2018/NMT-4331) projects.

[1] The authors are with the University Carlos III of Madrid, Department of Systems and Automation, Madrid, Spain. jgarciah@ing.uc3m.es scasa@ing.uc3m.es

[2] The authors are with the German Aerospace Center (DLR), Institute of Robotics and Mechatronics, 82234 Wessling, Germany. bernd.henze@dlr.de george.mesesan@dlr.de christian.ott@dlr.de

Because passivity theory can guarantee a robustness during interaction with the environment, this has been proven and integrated with whole-body control in others works. S. Fahmi et al. [5] presents a passive whole-body control method for quadruped robots that succeeds in dynamic locomotion while compliantly balancing the robot. The motion tracking takes into account the full-robot rigid body dynamics. We presented a passivity-based whole-body controller for humanoid robots in [6], which incorporates feedforward terms for following dynamic trajectories. The framework was combined in [7] with methods from the field of hierarchical multi-objective control to achieve a prioritization of tasks. The combined framework was adapted in [8] for operating humanoid robots in confined spaces, such as they occur in aircraft manufacturing.

On the other hand, in many robotic applications using manipulators, the desired Cartesian impedance behaviour is typically chosen as a kind of system similar to a mass-spring-damper. Some of these works are related to the design and application [9], [10]. Moreover, there are other works focused on the problem of implementing a dual-arm manipulation controller or even object balance manipulation [11], [12], [13], [14], [15]. Note that the field of dual-arm manipulation as well as balance control of legged robots suffers from the same challenge as pointed out in [16]. In both cases, the closed-kinematic chain arising from the multiple contacts of the feet with the floor or of the hands with the object causes a redundancy in the space of the contact wrenches, which is also known as the wrench distribution problem.

This paper combines our passivity-based whole-body controller from [6] with a dual-arm task in order to allow for bi-manipulation of an object while balancing the robot. For this purpose, the feedforward terms from [6] are adapted to preserve a good performance and robustness in the case of following a dynamic trajectory with the manipulated object. The final control architecture shows the structure of a PD+ controller [17] ensuring the stability and passivity of the closed-loop system.

As a result, we have developed a controller capable of performing balance and bi-manipulation tasks. This new system is equipped with various skills: First, the bi-manipulation task-oriented feedforward control allows making robust and efficient tracking in the movement of the transported object. Second, we have added the ability to distribute the load on the manipulator's arms according to the situation. We can decide which one holds the whole load or if the weight is distributed evenly, like in a collaborative task. Thus, the framework is able to solve the wrench distribution problem for the bi-manipulation and the balancing task. Third, we have provided the ability to readjust the bi-manipulation model according to the object to be grasped. And finally, the compliance controller allows continuing absorbing external disturbances.

The controller has been implemented and tested in different situations with the humanoid robot TORO [18], which demonstrates the performance and robustness of the proposed approach.

The paper is organized as follows. Section II summarizes the background related to the dynamical modelling of the robot. In Section III, the previous whole-body controller is described. Section IV describes further implementation details, such as the new bi-manipulation model estimating the object pose and the integration in the controller. Section V presents the experiments that validate the robustness of the new controller. Theses tests include the main skills of the tracking error performance, the application of the gamma parameter and the bi-manipulation and balancing behaviour against external perturbations. Section VI concludes the document, summarizing the achievements made and a proposal for the future.

II. MODELING

This section describes the dynamic model of the robot. This model will be used in the following section III to implement the dynamic model for the balance controller, which will be used to implement the bi-manipulation and balance controller in turn in section IV. The controller has the goal to use the end-effectors more specifically. On the one hand, the feet's end-effectors will be in contact with the ground to control the stability of the robot. And, on the other hand, the hands' end-effectors will be in contact with the bi-manipulated object, which will be influenced by the stability and the CoM of the robot. In this way, we can implement tasks where a humanoid robot would be able to transport large objects compliantly without the robot falling.

In more detail, for the whole-body humanoid robots, the use of dynamic models with a floating base is widespread. The reason is because they feature a higher flexibility regarding contact changes compared to dynamic models with a fixed base. In general, a central body within the kinematic structure of the robot is chosen as a base link, such as the trunk or the hip. Even the center of mass (CoM) is also used in some works as a base, since it represents an essential quantity for balancing.

Here, we will follow the notation of [6] by defining a CoM frame $\mathcal{C}$, which is located at the CoM and has the same orientation of the hip. Let $\boldsymbol{x}_c \in \mathbb{R}^3$ and $\boldsymbol{R}_c \in \mathcal{SO}(3)$ denote the position and orientation of the frame $\mathcal{C}$ with respect to the world frame $\mathcal{W}$. The corresponding translational and rotational velocities are $\dot{\boldsymbol{x}}_c$ and $\boldsymbol{\omega}_c$, respectively. Based on the n joint angles $\boldsymbol{q} \in \mathbb{R}^n$ and $\boldsymbol{v}_c = (\dot{\boldsymbol{x}}_c^T, \boldsymbol{\omega}_c^T)^T$, the dynamics of the humanoid robot is given by:

$$\boldsymbol{M}\begin{pmatrix}\dot{\boldsymbol{v}}_c\\ \ddot{\boldsymbol{q}}\end{pmatrix} + \boldsymbol{C}\begin{pmatrix}\boldsymbol{v}_c\\ \dot{\boldsymbol{q}}\end{pmatrix} + \underbrace{\begin{pmatrix}-m\boldsymbol{g}_0\\ \boldsymbol{0}\end{pmatrix}}_{\boldsymbol{g}} = \begin{pmatrix}\boldsymbol{0}\\ \boldsymbol{\tau}\end{pmatrix} + \boldsymbol{\tau}_{\text{ext}}. \quad (1)$$

Herein, $\boldsymbol{M} \in \mathbb{R}^{(6+n)\times(6+n)}$ and $\boldsymbol{C} \in \mathbb{R}^{(6+n)\times(6+n)}$ denote the inertia and Coriolis matrix, respectively. The gravitational torques are expressed by $\boldsymbol{g} \in \mathbb{R}^{6+n}$ with m denoting the overall mass of the robot and $\boldsymbol{g}_0 \in \mathbb{R}^6$ the gravitational acceleration. In this case, $\boldsymbol{g}_0$ is six-dimensional by containing also the rotational DoFs. The joint torques are described by $\boldsymbol{\tau} \in \mathbb{R}^n$. The influence of external wrenches on the robot is taken into account by the generalized torque vector $\boldsymbol{\tau}_{\text{ext}} \in \mathbb{R}^{6+n}$.

We separate the ψ end-effectors into two subgroups, the first one is referred to as "balancing end-effector" (*bal*) and contains the ψ_{bal} end-effectors that are used by the robot to support itself (usually the feet). The remaining $\psi_{\text{int}} = \psi - \psi_{\text{bal}}$ end-effectors are called "interaction end-effectors" (*int*), as they are still free to be used in a manipulation or interaction task (usually the hands). So, following this definition, the Cartesian velocities of the end-effectors $\boldsymbol{v} \in \mathbb{R}^{6\psi}$ are given by:

$$\boldsymbol{v} = \begin{pmatrix}\boldsymbol{v}_{\text{bal}}\\ \boldsymbol{v}_{\text{int}}\end{pmatrix} = \underbrace{\begin{bmatrix}\boldsymbol{Ad}_{\text{bal}} & \boldsymbol{J}_{\text{bal}}\\ \boldsymbol{Ad}_{\text{int}} & \boldsymbol{J}_{\text{int}}\end{bmatrix}}_{\begin{bmatrix}\boldsymbol{Ad} & \boldsymbol{J}\end{bmatrix}} \begin{pmatrix}\boldsymbol{v}_c\\ \dot{\boldsymbol{q}}\end{pmatrix} \quad (2)$$

with $\boldsymbol{v}_{\text{bal}} \in \mathbb{R}^{6\psi_{\text{bal}}}$ and $\boldsymbol{v}_{\text{int}} \in \mathbb{R}^{6\psi_{\text{int}}}$. The Adjoint matrix $\boldsymbol{Ad} \in \mathbb{R}^{6\psi\times 6}$ maps a motion of the CoM to the end-effectors while the Jacobian matrix $\boldsymbol{J} \in \mathbb{R}^{6\psi\times n}$ accounts for a motion of the joints. In the case where all external disturbances act solely at the end-effectors, $\boldsymbol{\tau}_{\text{ext}}$ simplifies to $\boldsymbol{\tau}_{\text{ext}} = \boldsymbol{J}^T\boldsymbol{F}_{\text{ext}}$.

III. BALANCING CONTROL

In [6], a passivity-based balancing control for torque-controlled humanoid robots was presented, which will be used as a basis for the bimanual control in the present paper.

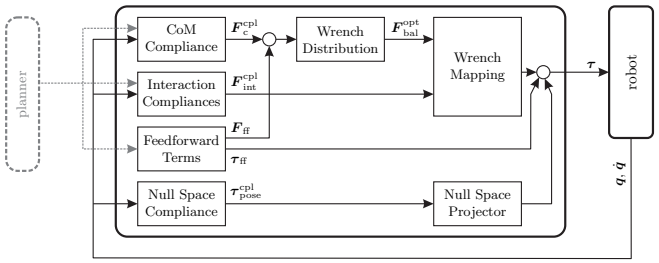

Fig. 2. Structure of the passivity-based balancing control from [6].

The balancing controller from [6] features several Cartesian compliances for stabilizing the center of mass frame $\mathcal{C}$ and the interaction end-effectors. An overview of the control approach is given in Figure 2. Note that the controller can utilize multiple contacts to support the robot, which creates a closed-kinematic chain involving the balancing end-effectors. The resulting redundancy in the space of the contact or balancing wrenches $\boldsymbol{F}_{\text{bal}}$ is also known as the Wrench Distribution Problem (WDP). In order to resolve the redundancy, the controller distributes the compliance wrench $\boldsymbol{F}_c^{\text{cpl}}$ (including gravity compensation $\boldsymbol{g}$) to the balancing end-effectors by solving a constrained quadratic optimization. Finally, the end-effector wrenches $\boldsymbol{F}_{\text{bal}}^{\text{opt}}$ and $\boldsymbol{F}_{\text{int}}^{\text{cpl}}$ are mapped to the control torques $\boldsymbol{\tau}$. The feedforward control is added to the feedback loop to improve the tracking behaviour. The resulting structure of the controller is similar to PD+ control, which allows us to prove stability and passivity of the closed-loop system [17], [19].

In order to derive the controller, a coordinate transformation is defined in [6], which replaces the joint velocities in the dynamic model (2) with the Cartesian coordinates of the end-effectors. Excluding singular configurations and redundant robots from our considerations, the transformation matrix $\boldsymbol{T}$ is defined by

$$\begin{pmatrix} \boldsymbol{v}_c \\ \dot{\boldsymbol{q}} \end{pmatrix} = \underbrace{\begin{bmatrix} \boldsymbol{I} & \boldsymbol{0} \\ -\boldsymbol{J}^{-1}\boldsymbol{A}\boldsymbol{d} & \boldsymbol{J}^{-1} \end{bmatrix}}_{\boldsymbol{T}^{-1}} \begin{pmatrix} \boldsymbol{v}_c \\ \boldsymbol{v} \end{pmatrix}. \tag{3}$$

Applying (3) to (1) leads to the transformed model

$$\boldsymbol{\Lambda} \begin{pmatrix} \dot{\boldsymbol{v}}_c \\ \dot{\boldsymbol{v}} \end{pmatrix} + \boldsymbol{\mu} \begin{pmatrix} \boldsymbol{v}_c \\ \boldsymbol{v} \end{pmatrix} + \boldsymbol{g} = \begin{bmatrix} -\boldsymbol{A}\boldsymbol{d}^T \\ \boldsymbol{I} \end{bmatrix} \boldsymbol{J}^{-T}\boldsymbol{\tau} + \boldsymbol{T}^{-T}\boldsymbol{\tau}_{\text{ext}} \tag{4}$$

with $\boldsymbol{\Lambda} = \boldsymbol{T}^{-T}\boldsymbol{M}\boldsymbol{T}^{-1}$, $\boldsymbol{\mu} = \boldsymbol{T}^{-T}\boldsymbol{C}\boldsymbol{T}^{-1} + \boldsymbol{T}^{-T}\boldsymbol{M}\dot{\boldsymbol{T}}^{-1}$ (Both $\boldsymbol{\Lambda}$ and $\boldsymbol{\mu} \in \mathbb{R}^{(6+n)\times(6+n)}$). The transformed model is reused in Sec. IV-A for integrating the bi-manipulation task.

However, this controller lacks to ability to manipulate a common object with both hands. In theory, the trajectories for both hands can be designed such that they stay in formation while moving the common object, but designing such a trajectory is rather cumbersome. Furthermore, the resulting stiffness and damping of the object can only be parameterized indirectly via the individual hand compliances. The same holds for the load distribution between the hands in case the robot is carrying a heavy object.

For this reason, a new controller has been developed that is capable of performing dual-arm manipulation by defining a Cartesian compliance for the common object instead of the individual hand compliance. the resulting object wrench is distributed to both hands by solving the closed kinematic chain of the upper body as detailed in the next section.

IV. BIMANIPULATION CONTROL

In this paper, we aim at integrating customized impedance control laws for dual arm manipulation into the whole-body controller from [6]. Based on the concept [15], we have developed a control system with abilities of balance and manipulation with two arms.

A. dual arm manipulation

As shown in the Figure 3, our approach is based on using two spring-dampers. This type of stiffness implementations allows adding the potential function, which is associated with the spatial spring. This characteristic, in turn, is closely related to the concepts of stability and passivity in closed-loop systems. Additionally, this impedance structure allows two different behaviours to be implemented. On the one hand, one behaviour defines the frame of the virtual object H_O, which depends on the end-effectors frames of the right H_R and left H_L arms [10]. This virtual object is connected through the spring-damper K_o to the virtual equilibrium position frame H_D, which depends on the CoM frames. In this way, we can control the movement of the grabbed object considering the impedance behaviour of the CoM. On the other hand, we can control the relative motion between the two arms (H_R, H_L) by adding the damper coupling K_c. In this way, we can control the distance between hands when the robot has to go to grasp an object or directly keeping the grip distance. Therefore, with K_o and K_c, we have defined an impedance behaviour which is useful for grabbing large objects with two hands.

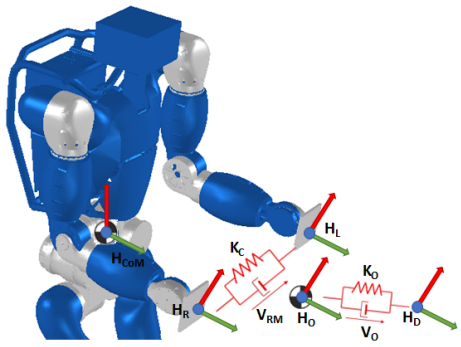

Fig. 3. Object and coupling compliance for dual-arm manipulation.

In Figure 3, the potential function for these two-arm impedance behaviours is defined by the Equation (5).

$$V(\theta) = V_S(H_O(H_R(\theta), H_L(\theta)), H_D(H_{CoM}(\theta)), K_o) + V_S(H_R(\theta), H_L(\theta), K_c) \tag{5}$$

The movement of the object can be obtained by the derivation of the Equation (5), as shown in [15]. This movement is represented by the object velocity wrench ($\boldsymbol{v}_o$ and $\boldsymbol{v}_{RM}$) and their relation to the hands' end-effectors velocity wrenches ($\boldsymbol{v}_R$ and $\boldsymbol{v}_L$) for the integration in the controller. In this case, we have defined the relationship between velocities through the transformation matrix $\tilde{\boldsymbol{T}}$. The corresponding transformation $\tilde{\boldsymbol{T}}$ is defined by:

$$\underbrace{\begin{pmatrix} \boldsymbol{v}_c \\ \boldsymbol{v}_{\text{bal}} \\ \boldsymbol{v}_o \\ \boldsymbol{v}_{\text{RM}} \end{pmatrix}}_{\begin{pmatrix} \tilde{\boldsymbol{v}}_c \\ \tilde{\boldsymbol{v}} \end{pmatrix}} = \underbrace{\begin{bmatrix} \boldsymbol{I} & \boldsymbol{0} & \boldsymbol{0} & \boldsymbol{0} \\ \boldsymbol{0} & \boldsymbol{I} & \boldsymbol{0} & \boldsymbol{0} \\ \boldsymbol{0} & \boldsymbol{0} & \gamma\,\boldsymbol{Ad}_{RO} & (1-\gamma)\,\boldsymbol{Ad}_{LO} \\ \boldsymbol{0} & \boldsymbol{0} & \boldsymbol{Ad}_{RO} & -\boldsymbol{Ad}_{LO} \end{bmatrix}}_{\tilde{\boldsymbol{T}}} \underbrace{\begin{pmatrix} \boldsymbol{v}_c \\ \boldsymbol{v}_{bal} \\ \boldsymbol{v}_R \\ \boldsymbol{v}_L \end{pmatrix}}_{\begin{pmatrix} \boldsymbol{v}_c \\ \boldsymbol{v} \end{pmatrix}} \quad (6)$$

where $\boldsymbol{v}_o \in \mathbb{R}^6$ is the velocity of the virtual object, $\boldsymbol{v}_{RM} \in \mathbb{R}^6$ is the relative speed between the end-effectors of the hands, $\boldsymbol{v}_R \in \mathbb{R}^6$ is the right hand velocity, $\boldsymbol{v}_L \in \mathbb{R}^6$ is the left hand velocity and $\gamma \in [0;1]$ is the load distribution factor. $\boldsymbol{Ad}_{RO} \in \mathbb{R}^{6\times6}$ and $\boldsymbol{Ad}_{LO} \in \mathbb{R}^{6\times6}$ are the Adjoint matrices between the right hand and the object and between the left hand and the object respectively.

As explained above, the final goal of the new controller is to achieve bi-manipulation and balance compliance for a humanoid robot using multiple contacts, while the passivity of the system is ensured. The implementation of the balance is maintained as in the previous version and has not been modified ($\boldsymbol{F}^{\text{opt}}_{\text{bal}}$). However, the remaining end-effectors behave according to the new described impedance behaviour.

For this, the bi-manipulation and balancing multi-contact controller is presented in two parts. First, the model in (4) is transformed into the task space to define the desired bi-manipulation and balancing behaviour. In order to obtain a representative new dynamic model, the Cartesian coordinates of the interaction end-effectors are replaced with the new task coordinates (in this case the grasped object $\boldsymbol{v}_o$ and $\boldsymbol{v}_{RM}$) through the transformation $\tilde{\boldsymbol{T}}$. Second, the controller is derived by employing the structure of the resulting equation of the new model to calculate the torque control $\boldsymbol{\tau}$.

With this model, the bi-manipulation part of the controller will be able to have various skills. Through K_o, the robot can control the object pose for handling tasks. Through K_c, the robot can perform tasks of approaching the hands towards the object and vice versa. The gamma parameter will allow distributing the object load in different ways between the arms. If the load is not uniform or ideally is not at the same distance from the hands' end-effector, the gamma factor can also help to compensate for this inequality.

Moreover, the compliance behaviour helps to absorb external disturbances on the robot. Finally, the model readjustment admits to achieving different tasks. For example, if the virtual object frame is inside of the hands, the task will be focused on transport. If the virtual object frame is outside of the hands, the task will be focused on sweeping.

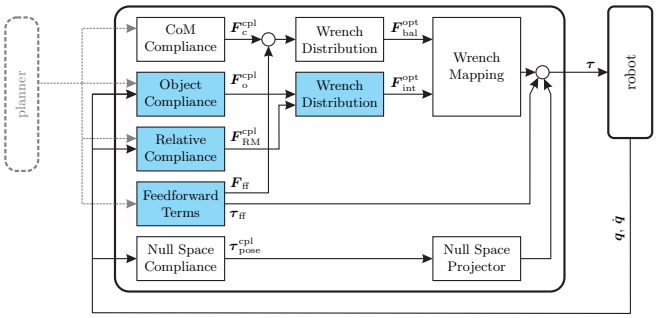

Fig. 4. Control architecture with the new wrench distribution system related to the dual-arm manipulation.

B. Integration into whole body controller

The bi-manipulation and balancing controller should be capable of stabilising a fixed equilibrium CoM point as well as following a given CoM and object trajectories at the same time. Now, the new control architecture is shown in Figure 4 and the controller requires the following information from the planner: the desired position $\boldsymbol{x}_c^d \in \mathbb{R}^3$ and orientation of the CoM frame $\mathcal{C}$. Also, it is necessary the desired position $\boldsymbol{x}_o^d \in \mathbb{R}^3$ and orientation $\boldsymbol{R}_o^d \in \mathcal{SO}(3)$ of the object and, of course, the desired position $\boldsymbol{x}_{RM}^d \in \mathbb{R}^3$ and orientation $\boldsymbol{R}_{RM}^d \in \mathcal{SO}(3)$ of the relative motion between the hands.

This controller is divided in two wrench distribution. The first one, the balance wrench distribution ($\boldsymbol{F}^{\text{opt}}_{\text{bal}}$) is computed by the force wrench of the CoM ($\boldsymbol{F}^{\text{cpl}}_{c}$) (through the CoM compliance) and the feedforward wrench ($\boldsymbol{F}_{ff}$) (through the Feedforward Terms). This feedforward wrench has been adapted to the new dynamic model. The second one, the object interaction wrench distribution ($\boldsymbol{F}^{\text{opt}}_{\text{int}}$) is calculated with the force wrench of the object ($\boldsymbol{F}^{\text{cpl}}_{o}$) (through the Object compliance) and the the force wrench of the relative motion ($\boldsymbol{F}^{\text{cpl}}_{RM}$) (through the Realtive compliance). The last part is a null space control (Null Space Compliance and Projector) and it is the same as the previous version.

Finally, the joint torques applied to the robot is a sum of three parts. a) The wrench mapping transforms the balance and object interaction wrenches ($\boldsymbol{F}^{\text{opt}}_{\text{bal}}$ and $\boldsymbol{F}^{\text{opt}}_{\text{int}}$) into torques. b) The Feedforward control also compute another part of the torques. And c) the Null Space control generates the third part of the torques (τ_{ff}). However, to undestand the calcutation of the joint torques to apply on the robot, firstly, we must obtain the dynamic model of the robot by applying the transformed model on the previous model (4) with matrix $\tilde{\boldsymbol{T}}$ in the new task space:

$$\tilde{\boldsymbol{\Lambda}} \begin{pmatrix} \tilde{\boldsymbol{v}}_c \\ \tilde{\boldsymbol{v}} \end{pmatrix} + \tilde{\boldsymbol{\mu}} \begin{pmatrix} \tilde{\boldsymbol{v}}_c \\ \tilde{\boldsymbol{v}} \end{pmatrix} + \tilde{\boldsymbol{T}}^{-T} \boldsymbol{g} = \tilde{\boldsymbol{T}}^{-T} \begin{bmatrix} -\boldsymbol{Ad}^T \\ \boldsymbol{I} \end{bmatrix} \boldsymbol{J}^{-T} \boldsymbol{\tau} + \tilde{\boldsymbol{\tau}}_{\text{ext}} \quad (7)$$

where $\tilde{\boldsymbol{\Lambda}} = \tilde{\boldsymbol{T}}^{-T} \boldsymbol{\Lambda} \tilde{\boldsymbol{T}}^{-1}$ and $\tilde{\boldsymbol{\mu}} = \tilde{\boldsymbol{T}}^{-T} \boldsymbol{\mu} \tilde{\boldsymbol{T}}^{-1} + \tilde{\boldsymbol{T}}^{-T} \boldsymbol{\Lambda} \frac{d}{dt} (\tilde{\boldsymbol{T}}^{-1})$. The generalised external forces are given by $\tilde{\boldsymbol{\tau}}_{\text{ext}} \in \mathbb{R}^{6+n}$. And $\boldsymbol{Ad}$ is the rotated grasp matrix, providing a mapping between the set of end-effectors wrenches and the total wrench at the CoM.

Taking in considerations deviations in velocity, position and orientation from the predefined trajectory, the desired closed-loop system behaviour is chosen:

$$\tilde{\boldsymbol{\Lambda}} \begin{pmatrix} \Delta\dot{\boldsymbol{v}}_c \\ \Delta\dot{\boldsymbol{v}}_{\text{bal}} \\ \Delta\dot{\boldsymbol{v}}_o \\ \Delta\dot{\boldsymbol{v}}_{\text{RM}} \end{pmatrix} + \tilde{\boldsymbol{\mu}} \begin{pmatrix} \Delta\boldsymbol{v}_c \\ \Delta\boldsymbol{v}_{\text{bal}} \\ \Delta\boldsymbol{v}_o \\ \Delta\boldsymbol{v}_{\text{RM}} \end{pmatrix} = \tilde{\boldsymbol{\tau}}_{\text{ext}} - \begin{pmatrix} \boldsymbol{F}_c^{\text{cpl}} \\ \boldsymbol{F}_{\text{bal}}^{\text{opt}} \\ \boldsymbol{F}_o^{\text{cpl}} \\ \boldsymbol{F}_{\text{RM}}^{\text{cpl}} \end{pmatrix} \tag{8}$$

If we compare (8) with (7), the identification of the required control law for the torques $\boldsymbol{\tau}$ is:

$$\tilde{\boldsymbol{T}}^{-T} \begin{bmatrix} -\boldsymbol{A}\boldsymbol{d}^T \\ \boldsymbol{I} \end{bmatrix} \boldsymbol{J}^{-T}\boldsymbol{\tau} = \tilde{\boldsymbol{\Lambda}} \begin{pmatrix} \dot{\boldsymbol{v}}_c^d \\ \dot{\boldsymbol{v}}_{\text{bal}}^d \\ \dot{\boldsymbol{v}}_o^d \\ \dot{\boldsymbol{v}}_{\text{RM}}^d \end{pmatrix} + \tilde{\boldsymbol{\mu}} \begin{pmatrix} \boldsymbol{v}_c^d \\ \boldsymbol{v}_{\text{bal}}^d \\ \boldsymbol{v}_o^d \\ \boldsymbol{v}_{\text{RM}}^d \end{pmatrix} + \boldsymbol{g} - \begin{pmatrix} \boldsymbol{F}_c^{\text{cpl}} \\ \boldsymbol{F}_{\text{bal}}^{\text{opt}} \\ \boldsymbol{F}_o^{\text{cpl}} \\ \boldsymbol{F}_{\text{RM}}^{\text{cpl}} \end{pmatrix} \tag{9}$$

Considering that $\boldsymbol{\tau}$ and $\boldsymbol{F}_{\text{bal}}^{\text{opt}}$ are the remaining free variables in (9), they can be determined in two steps using this equation. First, the task wrenches $\boldsymbol{F}_c^{\text{cpl}}$, $\boldsymbol{F}_{\text{bal}}^{\text{opt}}$, $\boldsymbol{F}_o^{\text{cpl}}$, and $\boldsymbol{F}_{\text{RM}}^{\text{cpl}}$ are calculated by representing the external load condition of the robot. Secondly, the control torque $\boldsymbol{\tau}$ is calculated by characterizing the internal load within the structure of the robot.

So, dividing in two parts the equation (9):

$$-\tilde{\boldsymbol{T}}^{-T}\boldsymbol{A}\boldsymbol{d}^T(\boldsymbol{J}^{-T}\boldsymbol{\tau}) = \tilde{\boldsymbol{\Lambda}}_1 \begin{pmatrix} \dot{\boldsymbol{v}}_c^d \\ \dot{\boldsymbol{v}}_{\text{bal}}^d \\ \dot{\boldsymbol{v}}_o^d \\ \dot{\boldsymbol{v}}_{\text{RM}}^d \end{pmatrix} + \tilde{\boldsymbol{\mu}}_1 \begin{pmatrix} \boldsymbol{v}_c^d \\ \boldsymbol{v}_{\text{bal}}^d \\ \boldsymbol{v}_o^d \\ \boldsymbol{v}_{\text{RM}}^d \end{pmatrix} - m\boldsymbol{g}_0 - \boldsymbol{F}_c^{\text{cpl}} \tag{10}$$

$$\tilde{\boldsymbol{T}}^{-T}(\boldsymbol{J}^{-T}\boldsymbol{\tau}) = \tilde{\boldsymbol{\Lambda}}_2 \begin{pmatrix} \dot{\boldsymbol{v}}_c^d \\ \dot{\boldsymbol{v}}_{\text{bal}}^d \\ \dot{\boldsymbol{v}}_o^d \\ \dot{\boldsymbol{v}}_{\text{RM}}^d \end{pmatrix} + \tilde{\boldsymbol{\mu}}_2 \begin{pmatrix} \boldsymbol{v}_c^d \\ \boldsymbol{v}_{\text{bal}}^d \\ \boldsymbol{v}_o^d \\ \boldsymbol{v}_{\text{RM}}^d \end{pmatrix} - \begin{pmatrix} \boldsymbol{F}_{\text{bal}}^{\text{opt}} \\ \boldsymbol{F}_o^{\text{cpl}} \\ \boldsymbol{F}_{\text{RM}}^{\text{cpl}} \end{pmatrix} \tag{11}$$

where we can describe $\tilde{\boldsymbol{\Lambda}} = [\tilde{\boldsymbol{\Lambda}}_1^T \tilde{\boldsymbol{\Lambda}}_2^T]^T$ and $\tilde{\boldsymbol{\mu}} = [\tilde{\boldsymbol{\mu}}_1^T \tilde{\boldsymbol{\mu}}_2^T]^T$ with $\tilde{\boldsymbol{\Lambda}}_1, \tilde{\boldsymbol{\mu}}_1 \in \mathbb{R}^{6\times 6+6\psi}$ and $\tilde{\boldsymbol{\Lambda}}_2, \tilde{\boldsymbol{\mu}}_2 \in \mathbb{R}^{6\psi\times 6+6\psi}$. Therefore, based on this new variables and comparing (10) and (11) without the common variable $\boldsymbol{J}^{-T}\boldsymbol{\tau}$ yields to:

$$\tilde{\boldsymbol{A}}\boldsymbol{d}^T \begin{pmatrix} \boldsymbol{F}_{\text{bal}}^{\text{opt}} \\ \boldsymbol{F}_o^{\text{cpl}} \\ \boldsymbol{F}_{\text{RM}}^{\text{cpl}} \end{pmatrix} = \underbrace{(\tilde{\boldsymbol{\Lambda}}_1 + \tilde{\boldsymbol{A}}\boldsymbol{d}^T\tilde{\boldsymbol{\Lambda}}_2) \begin{pmatrix} \dot{\boldsymbol{v}}_c^d \\ \dot{\boldsymbol{v}}_{\text{bal}}^d \\ \dot{\boldsymbol{v}}_o^d \\ \dot{\boldsymbol{v}}_{\text{RM}}^d \end{pmatrix} + (\tilde{\boldsymbol{\mu}}_1 + \tilde{\boldsymbol{A}}\boldsymbol{d}^T\tilde{\boldsymbol{\mu}}_2) \begin{pmatrix} \boldsymbol{v}_c^d \\ \boldsymbol{v}_{\text{bal}}^d \\ \boldsymbol{v}_o^d \\ \boldsymbol{v}_{\text{RM}}^d \end{pmatrix}}_{\text{feedforward}=\boldsymbol{F}_{ff}} - \underbrace{m\boldsymbol{g}_0}_{\text{gravity compensation}} - \underbrace{\boldsymbol{F}_c^{\text{cpl}}}_{\text{feedback}} \tag{12}$$

with $\tilde{\boldsymbol{A}}\boldsymbol{d} = \tilde{\boldsymbol{T}}\,\boldsymbol{A}\boldsymbol{d}\,\tilde{\boldsymbol{T}}^{-1}$. The right side of the Equation (12) can be interpreted as the general wrench that the controller needs to generate in the CoM for the stability task of the robot. It consists of a feedforward part, a gravity compensation and a feedback term as in PD+ control [17]. The left side of the equation is given by the wrenches of the end-effectors, which must be added to the desired wrench in the CoM.

However, there is an important detail. The transformed Adjoint matrix $\tilde{\boldsymbol{A}}\boldsymbol{d}$ in Equation (12) has 6 lines and $\boldsymbol{F}_{\text{bal}}^{\text{opt}}$ has a size of $6\psi_{\text{bal}}$. Therefore, $\boldsymbol{F}_{\text{bal}}^{\text{opt}}$ could not be directly obtained if there is more than one end-effector used for balancing ($\psi_{\text{bal}} > 1$). In order to resolve this force distribution problem caused by the redundancy in $\tilde{\boldsymbol{A}}\boldsymbol{d}$, the constrained quadratic optimization problem (used in [20]) is applied.

After determining the wrench distribution $\boldsymbol{F}_{\text{bal}}^{\text{opt}}$ for the balancing end-effectors, (11) can be used for computing the torque mapping:

$$\boldsymbol{\tau} = \underbrace{\boldsymbol{J}^T\tilde{\boldsymbol{T}}^T \left(\tilde{\boldsymbol{\Lambda}}_2 \begin{pmatrix} \dot{\boldsymbol{v}}_c^d \\ \dot{\boldsymbol{v}}_{\text{bal}}^d \\ \dot{\boldsymbol{v}}_o^d \\ \dot{\boldsymbol{v}}_{\text{RM}}^d \end{pmatrix} + \tilde{\boldsymbol{\mu}}_2 \begin{pmatrix} \boldsymbol{v}_c^d \\ \boldsymbol{v}_{\text{bal}}^d \\ \boldsymbol{v}_o^d \\ \boldsymbol{v}_{\text{RM}}^d \end{pmatrix} \right)}_{\text{feedforward}=\boldsymbol{\tau}_{ff}} - \boldsymbol{J}^T \begin{pmatrix} \boldsymbol{F}_{\text{bal}}^{\text{opt}} \\ \boldsymbol{F}_{\text{int}}^{\text{opt}} \end{pmatrix} \tag{13}$$

Note that the wrench distribution for the hands is given by

$$\boldsymbol{F}_{\text{int}}^{\text{opt}} = \begin{bmatrix} \gamma\,\boldsymbol{A}\boldsymbol{d}_{RO}^T & \boldsymbol{A}\boldsymbol{d}_{RO}^T \\ (1-\gamma)\,\boldsymbol{A}\boldsymbol{d}_{LO}^T & -\boldsymbol{A}\boldsymbol{d}_{LO}^T \end{bmatrix} \begin{pmatrix} \boldsymbol{F}_o^{\text{cpl}} \\ \boldsymbol{F}_{\text{RM}}^{\text{cpl}} \end{pmatrix} \tag{14}$$

based on (6). The parameter $\gamma \in [0, 1]$ determines the portion of $\boldsymbol{F}_o^{\text{cpl}}$ that is mapped to the right and the left hand, respectively.

V. EXPERIMENTAL EVALUATION

We performed experiments on various situations with the torque-controlled humanoid robot TORO [18]. The three presented experiments are the most appropriated to validate the new bi-manipulation and balance controller. Videos of the experiments presented in this section as well as of additional experiments can be found in the multimedia attachment.

TORO is a whole-body humanoid robot. Its weight is 76.4 kg and its height is 174 cm. This humanoid robot has 25 torque-controllable joints (six in each limb, and one for vertical torso rotation), 2 position-controlled joints in the neck, and is equipped with multiple sensors: position and torque sensors in each joint, an inertial measurement unit in the torso, force-torque sensors at the feet, and stereo and depth perception cameras in the head. The controller are implemented in Matlab/Simulink.

A. Tracking Error

The first set of experiments is focused on the performance of the bi-manipulation-oriented feedforward part of the controller. By varying the speed of the virtual object frame on the z-axis, it has been possible to verify the importance of this system within the controller and how tracking improves by adding the feedforward control. The most demanding experiment performed is shown in the Figure 5, where a displacement of the virtual object frame of 25 cm in 0.5 seg has been interpolated. In the upper graph, the feedforward control is deactivated. By contrast, in the lower graph, the system is activated. The black line represents the desired position of the object, the dashed red line represents the measured position of the object, and the blue line represents the tracking error.

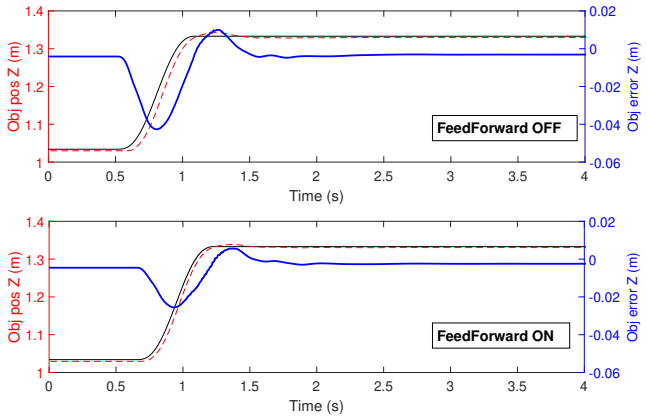

Fig. 5. Comparison of the object tracking error. Upper graph - FFWD deactivated. Lower graph - FFWD activated

In the lower part of the Figure 5, with the feedforward system activated in the controller, both tracking and position error improve by around 40%. The control compliance allows redistributing the forces. In this case, the CoM moves in the opposite direction to absorb the inertia of the movement and help in tracking. Therefore, we can validate the proposed bi-manipulation model and all the developed mathematics.

B. Gamma Parameter

The second set of experiments is focused on the operation of the gamma factor. In this case, a load of 4 kg has been placed on a bar that the robot grabs with both hands. The gamma parameter has taken these values [0.5 - 0.25 - 0.5 - 0.75] to verify the load distribution, while the position of the virtual object frame is kept. Changes in the gamma factor have been applied as a step response. Therefore, a large oscillation in the phases of change is shown in the graph. The continuous red line represents the force wrench of the right arm, the discontinuous red line represents the force wrench of the left arm, and the blue line represents the measured object position.

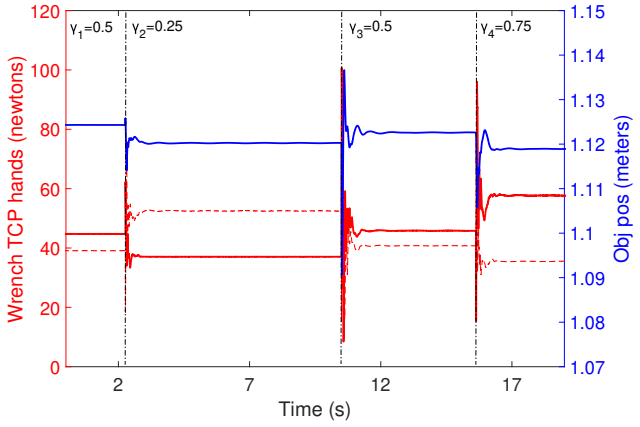

Fig. 6. TCP Force wrenches distribution. $\gamma = 0.5$ in $t = 0s$, $\gamma = 0.25$ in $t = 2s$, $\gamma = 0.5$ in $t = 10.5s$, $\gamma = 0.75$ in $t = 15.5s$.

The Figure 6 shows a correct and satisfactory force distribution on each of the hands end-effectors. When the gamma value is 25%, the highest force is made by the left arm. When the gamma value is 75%, the highest force is made by the right arm. At all times, the controller continues working to keep the object position. There is never an error bigger than 0.5 cm.

C. External Perturbation

The third set of experiments is focused on the behaviour of the controller against external disturbances. In this case, we want to verify the behaviour of the bi-manipulation system in two different ways. During the first part of the test, the computation of Vo is associated with CoM value. If the CoM moves due to external perturbations, the object will follow the same trajectory. During the second phase (after the second 12.5), the computation of Vo is associated with the value of the World frame. In this case, the World frame remains static at all times and therefore also the virtual object frame, independently of the external perturbations observed in the CoM. The Figure 7 shows the evolution of the three axes. The black line represents the desired object position, the discontinuous red line represents the measured object position, and the blue line represents the measured CoM position.

Figure 7 shows the behaviour of two essential parts of the bi-manipulation and balance controller. The first part checks if the controller is capable to perform a good object tracking. And the second part analyses if the controller absorbs disturbances in a compliant manner and then keep the balance. When $V_o = V_{CoM}$, the tracking of the virtual object frame is very robust, having errors below 2 cm. When $V_o = V_{world}$, the tracking is even better (below 1 cm). This type of test has also been proven by introducing trajectories of the CoM (walk) instead of disturbance. The obtained results have been very similar.

In addition to these experiments, other tests have been carried out where the efficiency and robustness of the new controller for trajectories of both V_o and V_{RM} have been verified while running the CoM trajectory at the same time.

VI. CONCLUSION

In this work, we have developed a balance and bi-manipulation whole-body controller that allows torque-controlled humanoid robots to be operated in multiple contact scenarios. The presented approach expands the previous work by (a) adding a bi-manipulation-oriented feedforward control to improve the performance of the tracking of the object, (b) exploiting multiple phases during the grip and handling process, and (c) allowing an extended task hierarchy by the interactions with objects and the environment while balancing.

Different experiments have been conducted with the humanoid robot TORO to confirm the features and performance of the proposed controller. The controller shows a good performance both in the regulation and in the tracking cases.

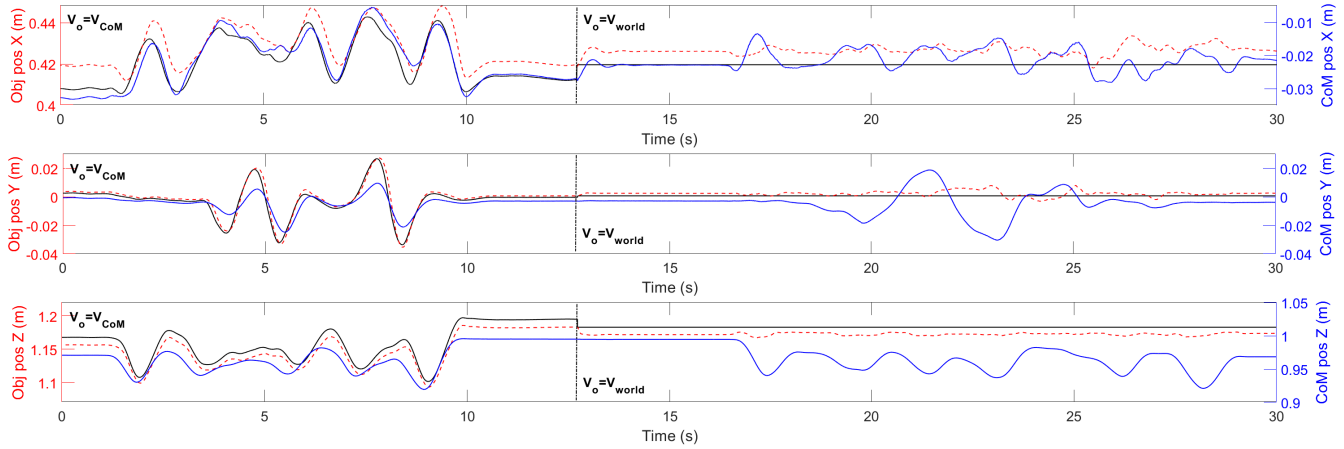

Fig. 7. Application of external perturbations in the CoM to validate the compliance control of the new dynamic model.

Therefore, with the new dynamic model integrated into TORO, we can validate that the bi-manipulation-oriented feedforward control is capable to make a robust and efficient tracking for the transported object trajectory. It is possible to distribute the grasped load on the manipulator's arms according to the situation. The readjustment of the bi-manipulation dynamic model is capable according to the type of grasped object. And, the compliance controller allows for absorbing external disturbances.

In the future, we plan to extend this bi-manipulation approach for different types of handled loads by adding adaptive control. When the humanoid robot TORO has to grab a new object with different characteristics of size, shape and weight, a new tracking error will appear. The control system must be able to adapt and correct this tracking error taking into account the balance at the same time.

References

[1] C. Ott, A. Albu-Schaffer, A. Kugi, and G. Hirzinger, "On the passivity-based impedance control of flexible joint robots," *IEEE Transactions on Robotics*, vol. 24, no. 2, pp. 416–429, 2008.

[2] N. A. Radford, P. Strawser, K. Hambuchen, J. S. Mehling, W. K. Verdeyen, A. S. Donnan, J. Holley, J. Sanchez, V. Nguyen, L. Bridgwater *et al.*, "Valkyrie: Nasa's first bipedal humanoid robot," *Journal of Field Robotics*, vol. 32, no. 3, pp. 397–419, 2015.

[3] C. Ott, C. Baumgärtner, J. Mayr, M. Fuchs, R. Burger, D. Lee, O. Eiberger, A. Albu-Schäffer, M. Grebenstein, and G. Hirzinger, "Development of a biped robot with torque controlled joints," in *2010 10th IEEE-RAS International Conference on Humanoid Robots*. IEEE, 2010, pp. 167–173.

[4] M. Neunert, M. Stäuble, M. Giftthaler, C. D. Bellicoso, J. Carius, C. Gehring, M. Hutter, and J. Buchli, "Whole-body nonlinear model predictive control through contacts for quadrupeds," *IEEE Robotics and Automation Letters*, vol. 3, no. 3, pp. 1458–1465, 2018.

[5] S. Fahmi, C. Mastalli, M. Focchi, and C. Semini, "Passive whole-body control for quadruped robots: Experimental validation over challenging terrain," *IEEE Robotics and Automation Letters*, vol. 4, no. 3, pp. 2553–2560, 2019.

[6] B. Henze, M. A. Roa, and C. Ott, "Passivity-based whole-body balancing for torque-controlled humanoid robots in multi-contact scenarios," *Int. J. Robotics Research*, vol. 35, no. 12, pp. 1522 – 1543, 2016.

[7] B. Henze, A. Dietrich, and C. Ott, "An approach to combine balancing with hierarchical whole-body control for legged humanoid robots," *IEEE Robotics and Automation Letters*, vol. 1, no. 2, pp. 700 – 707, 2016.

[8] B. Henze, A. Dietrich, M. A. Roa, and C. Ott, "Multi-contact balancing of humanoid robots in confined spaces: Utilizing knee contacts," in *IEEE/RSJ Int. Conf. on Intelligent Robots and Systems*, 2017, pp. 679 – 704.

[9] F. Caccavale, C. Natale, B. Siciliano, and L. Villani, "Six-dof impedance control based on angle/axis representations," *IEEE Transactions on Robotics and Automation*, vol. 15, no. 2, pp. 289–300, 1999.

[10] C. Natale, *Interaction control of robot manipulators: six degrees-of-freedom tasks*. Springer Science & Business Media, 2003, vol. 3.

[11] N. Vahrenkamp, D. Berenson, T. Asfour, J. Kuffner, and R. Dillmann, "Humanoid motion planning for dual-arm manipulation and re-grasping tasks," in *2009 IEEE/RSJ International Conference on Intelligent Robots and Systems*. IEEE, 2009, pp. 2464–2470.

[12] F. Zacharias, D. Leidner, F. Schmidt, C. Borst, and G. Hirzinger, "Exploiting structure in two-armed manipulation tasks for humanoid robots," in *2010 IEEE/RSJ International Conference on Intelligent Robots and Systems*. IEEE, 2010, pp. 5446–5452.

[13] J. M. Garcia-Haro, S. Martinez, and C. Balaguer, "Balance Computation of Objects Transported on a Tray by a Humanoid Robot Based on 3D Dynamic Slopes," in *2018 IEEE-RAS 18th International Conference on Humanoid Robots (Humanoids)*. IEEE, nov 2018, pp. 704–709.

[14] J. M. Garcia-Haro, E. Daniel Ona, S. Martinez, J. Hernandez-Vicen, and C. Balaguer, "Waiter Robot Application: Balance Control for Transporting Objects," in *2018 IEEE/RSJ International Conference on Intelligent Robots and Systems (IROS)*. IEEE, 2018, p. 5036.

[15] T. Wimböck, C. Ott, and G. Hirzinger, "Impedance behaviors for two-handed manipulation: Design and experiments," in *IEEE Int. Conf. on Robotics and Automation*, 2007, pp. 4182 – 4189.

[16] C. Ott, M. A. Roa, and G. Hirzinger, "Posture and balance control for biped robots based on contact force optimization," in *IEEE-RAS Int. Conf. on Humanoid Robots*, 2011, pp. 26 – 33.

[17] B. Paden and R. Panja, "Globally asymptotically stable 'PD+' controller for robot manipulators," *Int. J. of Control*, vol. 47, no. 6, pp. 1697 – 1712, 1988.

[18] J. Englsberger, A. Werner, C. Ott, B. Henze, M. A. Roa, G. Garofalo, R. Burger, A. Beyer, O. Eiberger, K. Schmid *et al.*, "Overview of the torque-controlled humanoid robot toro," in *2014 IEEE-RAS International Conference on Humanoid Robots*. IEEE, 2014, pp. 916–923.

[19] L. L. Whitcomb, A. A. Rizzi, and D. E. Koditschek, "Comparative experiments with a new adaptive controller for robot arms," *IEEE Trans. Robotics and Automation*, vol. 9, no. 1, pp. 59 – 70, 1993.

[20] G. Mesesan, J. Englsberger, G. Garofalo, C. Ott, and A. Albu-Schäffer, "Dynamic walking on compliant and uneven terrain using dcm and passivity-based whole-body control," *IEEE Robotics and Automation Letters (under review)*, 2019.